Gluing Nanoparticles with a Polymer Bonding Layer: The Strength of an Adhesive Bond

Baris Kokuoz, Konstantin G. Kornev,* and Igor Luzinov*

School of Materials Science and Engineering, Clemson University, 161 Sirrine Hall, Clemson, South Carolina 29634

ABSTRACT   The adhesive joint between silica nanoparticles and ultrathin poly(vinylpyridine) (PVP) layers (thickness between 3 and 100 nm) was tested using the cantilever of an atomic force microscope. Specifically, the strength of the adhesive bond (or practical adhesion) was probed in a tearing contact mode, when the particle was removed by applying a tangential force parallel to the substrate surface. The effect of the polymer molecular weight and layer thickness on the particle (practical) adhesion was investigated. It was found that the particles were removed by destroying the cohesive contact zone and that the PVP layer thickness had a pronounced effect on the force needed to destroy the adhesive joint. In particular, the greater the layer thickness, the larger was the required break force. However, the strength of the adhesive joint was estimated to be higher for a thinner layer. It is suggested that mechanical properties of the system as well as molecular characteristics of the PVP layer are responsible for the trend observed. The molecular weight of the polymer did not significantly affect the strength of the adhesive bond.

KEYWORDS: adhesion • nanoparticles • AFM • poly(vinylpyridine) • adhesive joint • thin polymer layer

INTRODUCTION

In engineering assemblies, adhesive joints are used for gluing together secondary noncritical parts of an assembly, where the load is transferred through interfacial shear (1). The use of the adhesive bonding is limited for primary structural applications because of strength and reliability issues. However, because engineering structures and devices have become progressively smaller, mechanical methods such as nuts, bolts, washers, and shims that join the components have become almost impossible to use. Welding and soldering are also problematic because the local heating may potentially destroy the integrity/properties of the nano- and microobjects being assembled. Therefore, it is attractive to assemble structures/devices by gluing small parts together with ultrathin adhesive layers. In order to develop this nanotechnology further, one needs to know the critical factors that control the strength and reliability of adhesive bonds.

One of the primary building blocks for future nano- and microdevices/structures consists of particles with diameters on the submicron level or nanoparticles. The anchoring of colloidal nanoparticles onto a substrate can be accomplished by surface modification with functional groups that are attractive to the particles. For instance, functional groups such as thiols are often used to immobilize nanoparticles on various oxide surfaces (2, 3). Various silanes also have been employed for this purpose (4). Poly(vinylpyridine) (PVP) has been used as an effective polymer adhesive to immobilize nanoparticles as well (5, 6). The advantage of a polymeric adhesive is in the fact that each macromolecule provides many binding sites for simultaneous interaction with the nanoparticle and substrate. This cooperative interaction results in strong binding of the nanoparticles.

In the preceding publications, the potential of PVP as a material for the creation of a bonding nanolayer was clearly demonstrated. However, the actual strength of the adhesive bond between the particles and the PVP film was not measured. In particular, neither the PVP molecular weight nor the thickness of the film were varied, so that the influence of these factors on the particle bonding is not well understood. In the present study, focus is placed on the estimation of the strength of the adhesive bond and the effects of the molecular weight and film thickness on the adhesive properties of PVP layers. Specifically, the strength of the adhesive joint was probed in a tearing contact mode, when a particle was removed by applying a tangential force parallel to the substrate surface.

We have used atomic force microscopy (AFM) to evaluate the strength of the adhesive joint. This method has already been used for the manipulation of the nanosize particles on different surfaces (7–10). In fact, using an AFM tip, one can apply normal and lateral loads to different substrates and actually measure the reaction forces. This allows one to probe different substrate properties, for example, adhesion and friction properties of the tip/substrate pairs. For instance, Eppler et al. showed that a small area of the surface can be cleared of the adsorbed particles by deliberately increasing the applied force to the surface and scanning the surface (11). Yang and Sacher used the same principle to mechanically push oxidized copper clusters on a polymer surface and then to assemble them into a cluster line at the edges of the scan area (12).

Recently, the same method was successfully employed, quantitatively, for the detachment of cells, such as bacterial cells, using an AFM cantilever (13, 14). In the present study,

---

we suggest that this same AFM technique could be employed for the removal of individual nanoparticles anchored to a surface via the thin polymer film and, hence, could allow quantification of the strength of their adhesive bonding to the films. Specifically, the stress needed to break the adhesive joint, involving silica nanoparticles and PVP, could be estimated experimentally. This stress is typically referred to as a practical adhesion (15). This type of characterization is important to direct the selection of "nanoadhesive" systems for micro- and nanodevices/structures. To the best of our knowledge, the results presented here are the first attempt to correlate the strength of the ultrathin, (macro)molecular level adhesive joints with the thickness and molecular characteristics of a polymer bonding layer.

EXPERIMENTAL SECTION

Materials and Samples. Silicon wafers (MEMC Electronic Materials Inc., St. Peters, MO) were cut into strips (1 cm × 3 cm) and cleaned in an ultrasonic bath for 30 min. Prior to coating, all samples were subjected to a standard Piranha solution treatment ($H_2O_2/H_2SO_4 = 1/3$). **Caution!** *Piranha solution is highly corrosive and extremely reactive with organic substances. Gloves, goggles, laboratory coat, and face shields are needed for protection.* Treated samples were rinsed with deionized water and stored in water until the coating process with poly(2-vinylpyridine) (PVP) in a clean room. Immediately prior to coating, the wafers were dried under a stream of nitrogen.

PVP of three different molecular weights (37 000, 121 000, and 159 000 g/mol) was used in the study. Polymer solutions were prepared, at different concentrations, by dissolving PVP (Sigma-Aldrich Inc., St. Louis, MO) in methyl ethyl ketone (Mallinckrodt Baker Inc., Phillipsburg, NJ), and these solutions were stored in sealed bottles. Cleaned and piranha-solution-treated silicon wafers were then dip-coated (Mayer Fientechnik D-3400) using the solutions to achieve an ultrathin PVP film. Applied coating thicknesses were measured by a one-wavelength ellipsometer and were found to range between 3 and 100 nm. Ellipsometry was performed with a COMPEL discrete polarization modulation automatic ellipsometer (InOmTech, Inc.) at a 70° angle of incidence. Original silicon wafers from the same batch were tested independently and were used as reference samples for the analysis of deposited polymer layers. A refractive index of 1.5 was used to calculate the thickness of the PVP layers.

Silica nanoparticles (Polysciences Inc., Warrington, PA) were deposited from water under ultrasonic agitation onto the surface of the silicon wafers covered with the PVP films. A suspension of the particles in water (approximately 5 wt %, as obtained from the supplier) was diluted 150 000 times in deionized water and used for deposition. The wafers were placed face down into a concave glass beaker, with edges-only contact to protect the surface from damage, and sonicated for 5 min. This method provided adsorption of the individual particles onto the surface without agglomeration. The samples were observed using a field emission scanning electron microscope, Hitachi S4800, equipped with an Oxford INCA Energy 200 energy-dispersive spectrometer and a GW Electronics Centaurus backscatter detector. Scanning electron microscopy analysis revealed that the diameter of the adsorbed nanoparticles was 128 ± 54 nm.

Atomic Force Microscopy (AFM). In the present study, contact-mode AFM (Digital Instruments NanoScope IIIa, Veeco, Plainview, NY) was utilized to determine the strength of the adhesive joint formed between the silica particles and the ultrathin PVP films. The measurements were conducted in ambient air at room temperature. The inclination angle of the cantilever long axis with respect to the surface was about 10°

(16). For measurements involving thinner PVP layers, a contact-mode silicon nitride cantilever with a pyramidal tip (model DNP-20; Veeco Instruments, Plainview, NY) was used to scan a certain area of the surface (10 μm × 10 μm) with a scan angle of 0°, making it possible to avoid twisting of the tip and limiting the scan to the bending movement. The force spring constant for the tips was on the level of 0.1−0.6 N/m. The scan rate was kept constant at the 1 Hz level.

In cases where the PVP layer thickness was increased (above 10−15 nm), the above-mentioned silicon nitride tips were found to be inadequate for removing particles because of their low force constants. Therefore, a second set of stiffer AFM cantilevers, NSC 11 series silicon cantilevers (with conical tip) from MikroMasch USA (San Jose, CA), was employed. The force spring constant for these tips was on the level of 1.5−5 N/m. The tips were also heat-treated to increase their radii. (Employment of the original tips, which had radii of 10−20 nm, resulted in scratching of the PVP films during measurements).

To increase the tip radius, the cantilevers were placed into a preheated oven at 850 °C for 2.5 h. Field emission scanning electron microscopy (FESEM) images (not shown) indicated that the tip radii increased to 100−150 nm after this heat treatment. The treated cantilevers were coated with gold on one side with a gold sputter to improve light reflection during the AFM scanning. While the weight change was controlled using a quartz resonance microbalance, 25 nm of gold was coated onto the tips. Tips were adhered to a microscope slide and "sandwiched" with another slide. In this way, the tips were protected and a minimal area was exposed to the gold (providing less mechanical interference due to weight change).

For measurement of the force required for detachment of a particle from the wafers covered with a PVP layer, the procedures described in refs 13 and 14 were followed. The force applied by the tip to the surface was calculated using force−calibration curves. Force−calibration curves were obtained for all samples on a particle-free area, before and after the removal of silica particles. Surface contact forces (normal) applied by the cantilever were calculated using Hooke's law, in the form

$$F = k\Delta x \tag{1}$$

where k is a cantilever spring force constant and Δx is tip deflection determined using the method suggested in the Digital Instruments instruction manual (16). The sensitivity was set before the capture of each force−calibration curve by drawing a parallel to the retracting line. The captured images were then processed to obtain the Δx value.

The cantilever spring (force) constant, k, was found by testing a standard cantilever against the Si_3N_4 cantilever with a known force constant supplied by Microscope Inc. (model CLFC-NOMB). A detailed description of this method is given by Tottonese and Kirk (17). In brief, a SiN_4 or silicon cantilever was tested against a cantilever of a known force constant as a reference cantilever, and the deflection was recorded. The cantilever was then tested against a surface (a clean silicon wafer) infinitely harder relative to the cantilever compliance. As shown in ref 17, the force constant of the cantilever can be calculated as

$$k_{test} = k_{ref}(\delta_{tot} - \delta_{test})/(\delta_{test} \cos \theta) \tag{2}$$

where k_{ref} is the force constant of the reference cantilever, δ_{tot} is the cantilever deflection against the wafer, δ_{test} is the cantilever deflection against the reference cantilever, and θ is the angle between the cantilever under test and the reference cantilever (10° in this study).
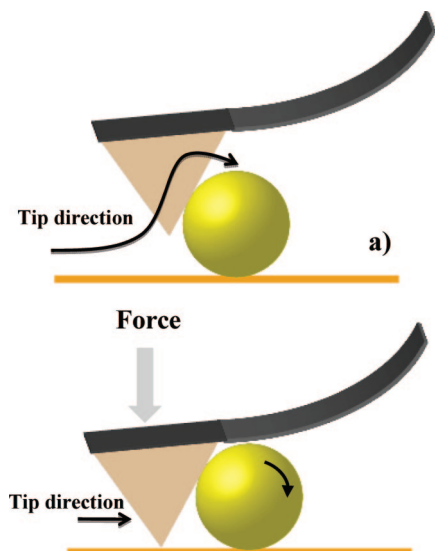
FIGURE 1. Schematic of AFM operation in the contact mode on the surface covered with nanoparticles: under minimal (a) and excessive force (b). The sketch is not to scale: the size of the particle is exaggerated.

To quantify the force required to detach particles from the PVP thin films, the relationship between the applied force **F** and the deflection set point was independently established for each sample analyzed. Normal force $\mathbf{F_y}$ was calculated by adding the value of the tip—substrate adhesion force, $\mathbf{F_a}$ determined from force—distance curves for each cantilever and sample, to **F**:

$$\mathbf{F_y} = \mathbf{F_a} + \mathbf{F} \qquad (3)$$

Once the force—calibration curves are obtained for a force range on a small and particle-free area (1 μm × 1 μm) over a range of force values, the relative strength of the adhesive bond for either one particle or several particles in an area can be determined.

Following force—calibration of the AFM, a minimum of two samples was prepared for each thickness and three measurements were taken randomly from those samples to show the method reproducibility and to make the measurements statistically representative. A new tip was used for every measurement. Scanning of the selected area was started with a low setpoint voltage (i.e., low surface force) and increased by 0.25 V increments. AFM images were captured for each increment and further compared with one another. Scanning was stopped when 100% removal of the particles was achieved before reaching instrument limits.

RESULTS AND DISCUSSION

Mechanical Analysis for the Detachment of the Particles with the AFM Cantilever. In our measurements, an AFM cantilever was used to scan (in the contact mode) a certain area of the surface with a scan angle of 0°, making it possible to avoid twisting of the tip and limiting the scan to the bending movement. The bending moment of the cantilever is proportional to the reaction force exerted by the substrate surface or obstacle. If the surface contact force is small, the tip simply slips over the particle (Figure 1a). If the applied force is high enough to overcome the strength of the adhesive bond for an attached particle, it causes the particle to detach and move. In this
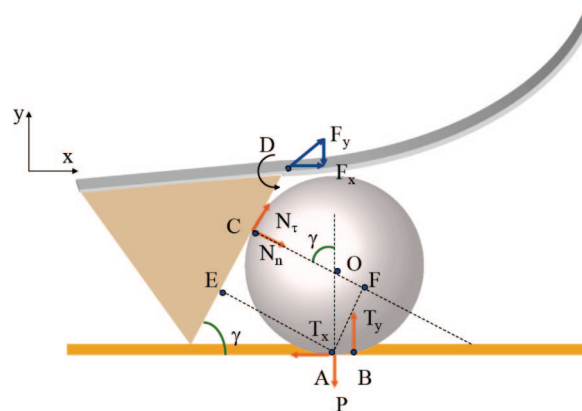

FIGURE 2. Mechanical schematic for detachment of the particles with the AFM cantilever. The schematic is not to scale: the size of the particle and thickness of the polymer bonding layer are exaggerated.

manner, the particles are *swept away* or *torn off* by the tip to the edges of the scanned area (Figure 1b).

The strength of the adhesive joint between a silica nanoparticle and the silicon wafer, via a PVP bonding layer, *Ad*, can be estimated as

$$Ad = \mathbf{P}/S \qquad (4)$$

where **P** is the normal force needed to destroy the adhesive bond and *S* is the contact area between the nanoparticle and the bonding polymer layer.

For the AFM experiments reported in this work, the force applied to the nanoparticle, and thus to the nanoparticle/polymer interface, can be expressed through the vertical and horizontal components of the force applied to the cantilever. Full mechanical analysis is quite complicated, and here we will only sketch the idea to illustrate the importance of a new physical parameter, the torque arm. The full theory behind the proposed method of nanolayer characterization deserves a separate paper and will be published elsewhere.

The detachment of a nanoparticle, revealed via its movement, can be realized via two competitive modes: rolling and sliding. In general, the sliding always requires higher forces than the rolling (18, 19). As recognized long ago (see, for example, reviews given in refs 18 and 19) to ensure sliding, one needs to satisfy certain conditions on applied forces. In particular, the torque on the particle must be zero. In most cases, this condition cannot be met in experiments. It is suggested (from the schematic in Figure 2) that torque on the particle is definitely present in our system and the rolling mode is in effect in our measurements.

Another specific feature of our system is that the polymer bonding layer is compliant. Therefore, because of the physical deformation of the adhesive layer, we have to distinguish points A and B, where the horizontal reaction force $\mathbf{T_x}$ (and force **P**) and vertical reaction force $\mathbf{T_y}$ have been applied (see the schematic in Figure 2). The distance |AB| can be found by solving a contact problem of elasticity or viscoelasticity. Some solutions for macroscopic layers are given in the book by Johnson (18). The short-range chemical interactions

between the particle surface and the polymer nanolayer can be accounted for by the specific boundary conditions for elasto(plastic) contact. Therefore, the solution of this contact problem provides the dependence of the shift $|AB|$ on the material interfacial parameters of the particle/nanolayer pair. In our phenomenological model, the characteristic length scale $|AB|$, the torque arm is considered as a physical parameter of the given pair of materials (19). Moreover, focusing only on the particle/nanolayer pair, we assume that the reaction force $\mathbf{N}_n$ is proportional to the normal force $\mathbf{F}_y$. Therefore, the problem is thus reduced to finding a relationship between the reaction force $\mathbf{N}_n$ and the force required to destroy the adhesive bond, $\mathbf{P}$.

The cantilever in our model is replaced by an equivalent system of forces, normal reaction force $\mathbf{N}_n$ and tangential reaction force $\mathbf{N}_\tau$. We consider $\mathbf{N}_n$ to be positive when it points down and $\mathbf{N}_\tau$ to be positive when it points up (see the notations in Figure 2). The projections of the normal and tangential forces $\mathbf{N}_n$ and $\mathbf{N}_\tau$ on the x and y directions read

$$\mathbf{N_x} = \mathbf{N_n} \sin \gamma + \mathbf{N_\tau} \cos \gamma \tag{5}$$

$$\mathbf{N_y} = -\mathbf{N_n} \cos \gamma + \mathbf{N_\tau} \sin \gamma \tag{6}$$

Therefore, the balance of forces acting on the particle is written as

$$\mathbf{N_n} \sin \gamma + \mathbf{N_\tau} \cos \gamma - \mathbf{T_x} = 0 \tag{7}$$

$$-\mathbf{N_n} \cos \gamma + \mathbf{N_\tau} \sin \gamma + \mathbf{T_y} - \mathbf{P} = 0 \tag{8}$$

and the torque balance with respect to point A gives (we pick the counterclockwise rotation as positive):

$$\mathbf{T_y}|AB| - \mathbf{N_\tau}|AE| - \mathbf{N_n}|AF| = 0 \tag{9}$$

From these equations, we can find a relationship between the adhesive force $\mathbf{P}$ and the applied force ($\mathbf{N}_n$, $\mathbf{N}_\tau$). Indeed, expressing the reaction force $\mathbf{T}_y$ from (8), we get

$$\mathbf{T_y} = \mathbf{P} + \mathbf{N_n} \cos \gamma - \mathbf{N_\tau} \sin \gamma \tag{10}$$

Introducing the friction coefficient K as $\mathbf{N}_\tau = K\mathbf{N}_n$, we obtain

$$\mathbf{T_y} = \mathbf{P} + \mathbf{N_n}(\cos \gamma - K \sin \gamma) \tag{11}$$

From (9), we thus find

$$\mathbf{P} = \mathbf{N_n}[(K|AE| + |AF|)/|AB| - (\cos \gamma - K \sin \gamma)] \tag{12}$$

or using the geometrical relationships, we express $\mathbf{P}$ as

$$\mathbf{P} = \mathbf{N_n}\left\{\frac{|OC|}{|AB|}[K(1 + \cos \gamma) + \sin \gamma] - (\cos \gamma - K \sin \gamma)\right\} \tag{13}$$

where $|OC|$ is the particle radius. Typically, the ratio $|OC|/|AB|$ is much greater than 1; hence, the force required to destroy the adhesive bond and measured with AFM scales as $[\mathbf{P}] \sim [\mathbf{N}_n]|OC|/|AB|$. On the other hand, for a thin layer, one can assume that the torque arm $|AB|$ is proportional to the film thickness. From these scaling arguments and suggesting that $\mathbf{N}_n \sim \mathbf{F}_y$, we conclude that, for the same $\mathbf{F}_y$ applied in our experiment, force $\mathbf{P}$ is higher for the thinner bonding polymer layers. However, as the film thickness increases, the parameter $|AB|$ would deviate from the linear dependence on the film thickness, approaching some finite value as the thickness goes to infinity (18).

Adhesive and Cohesive Failure of the Adhesive Bond. There are two major types of failure for the adhesive bond under consideration in this work: adhesive and cohesive. The adhesive failure is observed through the simple delamination of the particle from the PVP bonding layer. In addition, the adhesive failure is detected if delamination of the polymer layer from the silicon wafer is found during particle removal. If the strength of the particle−PVP and substrate−PVP adhesive interactions is higher than the strength of the PVP layer, a cohesive failure of the layer is observed. In this case, the macromolecular bonding layer is destroyed in a tearing mode because of the rolling of the nanoparticle by the AFM cantilever.

Morphology of the Sample Prior to Adhesive Measurements. Figure 3a shows an FESEM image of the surface after SiO$_2$ particle adsorption. Evidently, nanoparticles had adsorbed with minimal agglomeration and were discretely dispersed on the surface. Figure 3b illustrates a side view of the same surface. Image analysis shows that the nanoparticles were resting on the surface of the PVP film and were slightly rather than deeply incorporated into the film. An average of 54 ± 26 particles per scanned area (10 μm $\times$ 10 μm) with 128 ± 54 nm diameter was found on the samples. Cross-sectional AFM analysis of the coatings (results are not shown) revealed a smooth and flat thin film covered with nanoparticles, with no significant surface irregularities apparent.

Morphology of the Sample Following Adhesive Measurements. We successfully employed contact-mode AFM to remove the adsorbed particles from PVP ultrathin films (Figure 4). Film deformation and height differences were observed at places where the removed particles had been previously located. AFM imaging and cross-sectional analysis showed a "hump" formation on the polymer surface, as shown in Figure 5. This kind of formation was observed on all surfaces, regardless of the coating thickness or molecular weight. It appears that, during the removal, polymeric chains elongate to break and then leave behind debris that form these humps. The measured height and vertical distance of the humps were 7 ± 2 and 191 ± 36 nm, respectively. The size of the hump was virtually the
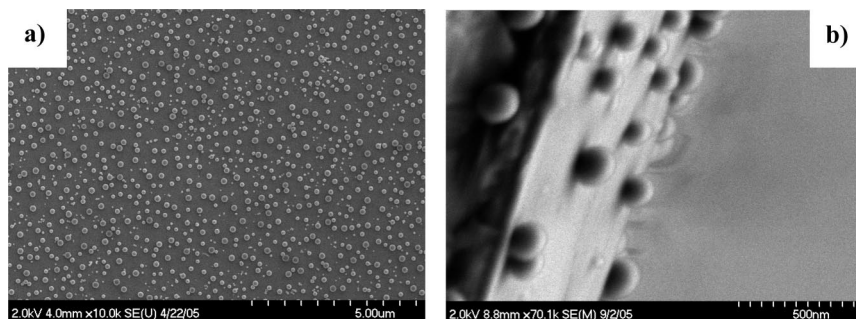
FIGURE 3. (a) FESEM image of the surface covered with silica particles. (b) Side view (90°) of the surface covered with silica particles. The thickness of the PVP layer is 12 nm.
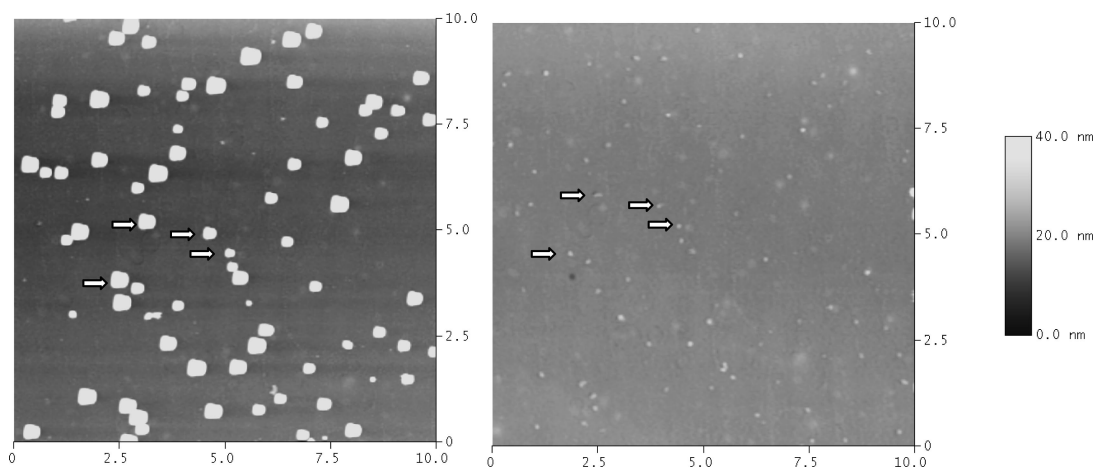

FIGURE 4. AFM images of the surface before (left) and after (right) particle removal. Arrows show the particle locations before and after removal. The positions of the "humps" can be observed on the right image. Image size: 10 μm × 10 μm. The particles appear not round because of employment of the blunted tip for the imaging.
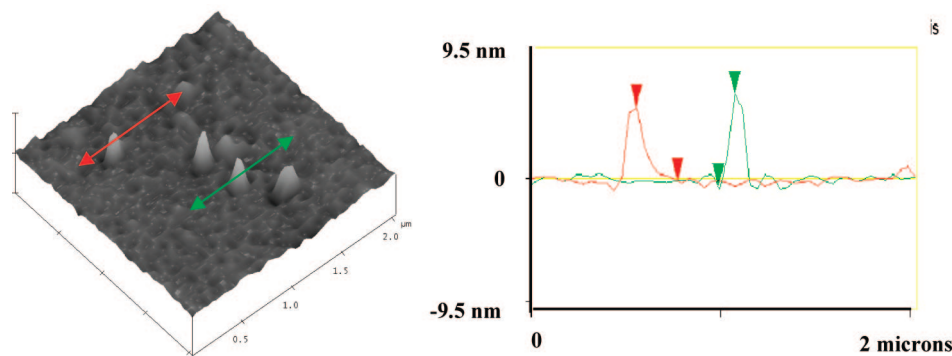
FIGURE 5. Three-dimensional (2 μm × 2 μm) and cross-sectional AFM images of the "humps" formed in the PVP bonding layer after the particles were removed by the AFM cantilever.

same for all of the different samples and did not clearly correlate with either the thickness or molecular weight of the PVP layer. Lateral dimensions of the hump were comparable with the diameter of the particles anchored. The modest widening of the dimensions can be presumed to be due to the AFM tip contribution, which can be estimated as adding 20–30 % of the total width. The formation of the hump points toward a conclusion that the failure of the adhesive joint occurs in the PVP film, within a certain distance from the particle. It has definitely indicated that the particles were not simply delaminated from the polymer layer but rather that the macromolecular bonding layer was destroyed. Thus, a cohesive failure, where the strength of the particle–PVP and substrate–PVP adhesive bond was

higher than the strength of the PVP film, was observed. The polymer bonding layer was destroyed in a tearing mode because of the rolling of the nanoparticle by the AFM cantilever.

One of the concerns about using the "push-out" technique was the possibility for disruption of the polymer surface during imaging in contact mode with a sharp and stiff tip (20). Following the removal experiments, the edges of the cleaned areas were examined with AFM and FESEM. No evidence was found for surface damage, and no ridge formation was observed at the edges. A clear demonstration of a cleaned area was obtained with FESEM, where the scan size was increased to 30 μm instead of 10 μm, making it easier to find the cleaned area under the electron micro-
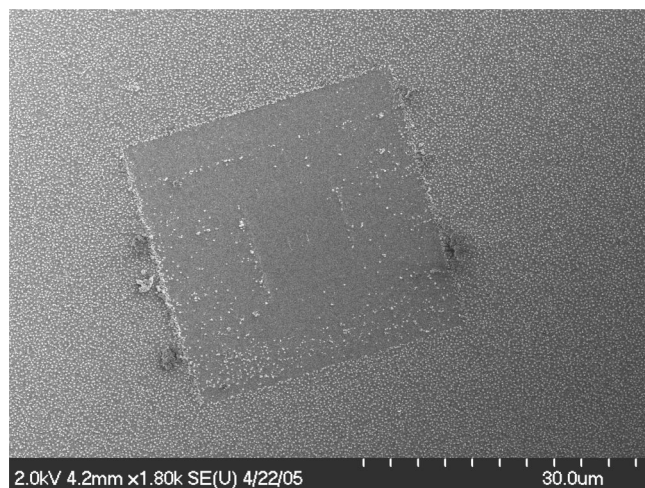
FIGURE 6. FESEM image of the surface after particle detachment. Cluster formation on the edges is noticeable.
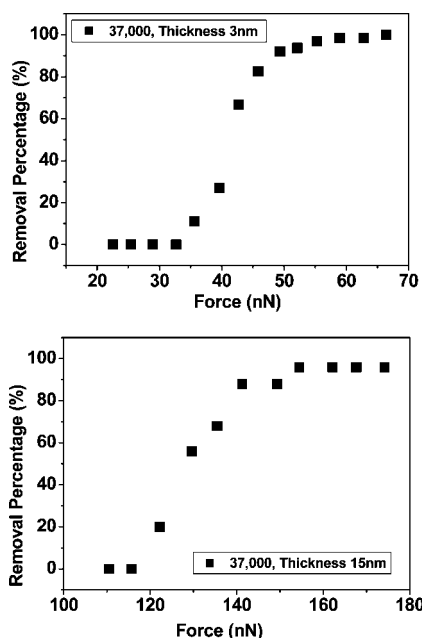

FIGURE 7. Nanoparticle removal percentage versus force F_y applied to a nanoparticle/PVP layer. Thickness of the PVP layer: 3 and 15 nm. PVP molecular weight: 37 000 g/mol.

scope. In Figure 6, detached particles and clusters formed on the edges in the $x-y$ direction are visible. In addition, Figure 6 indicates the presence of a polymeric material within the clusters of the particles. This observation supports the suggestion that, in fact, the PVP bonding layer is destroyed cohesively during particle removal as a result of the adhesive AFM measurements.

Results of Adhesive Measurements. Figure 7 shows the typical removal percentage versus applied force dependency for samples with two different film thicknesses prepared from PVP of the same molecular weights. It is clear that the forces required to detach the particles varied depending on the coating thickness. The plot shows an S-type curve with a steep increase in the number of particles detached in the range of 20−80%. The distribution in the values of the forces measured can be connected to the polydispersity of the particles. Another reason is the distri-
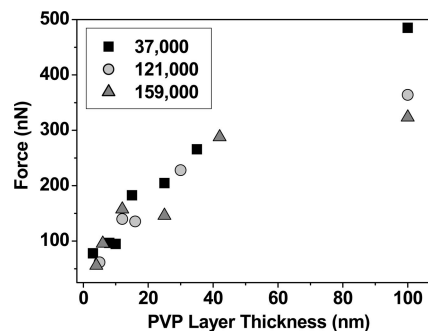

FIGURE 8. Force F_y required for detaching 100% of the silica particles versus thickness of the PVP bonding layer. 100% detachment was not achieved with the 100-nm-thick layers for all three molecular weights. The percent detachment values for 100 nm coating thickness were 30, 89, and 49% for polymers with molecular weights of 37 000, 121 000, and 159 000 g/mol, respectively.

bution of the actual angles at which the tip of the cantilever hits the particles. Nevertheless, the above experimental data can be used to estimate the reliability of the polymeric adhesives for component assembly.

The dependence of the required force to detach 100% of the particles on the coating thickness is shown in Figure 8. For all three molecular weights, the force increased with the layer thickness almost linearly. [It is necessary to highlight that 100% detachment was not achieved with the 100-nm-thick layers for all three samples possessing different molecular weights of the PVP.] This behavior may be attributed to the increased contact area between the particles and the PVP film. Specifically, when a particle is forced into contact with the PVP film during agitation of the colloidal system in an ultrasonic bath, the particle, being stiff, may partially penetrate into the macromolecular bonding layer upon impact. As the thickness of the "soft" PVP film increases, the penetration may become more pronounced, thus increasing the contact area between the particle and the polymer layer.

To confirm this hypothesis, the AFM images of the surfaces prior to removal were further processed with respect to their bearing depth. The bearing depth was estimated by employing the standard NanoScope (Veeco) software utilized for AFM image analysis. The bearing depth is defined as the distance from the highest point of the highest nanoparticle within the image area to the surface of the PVP layer. In other words, the distance from the top of the tallest particle to the point where the particle is sitting in contact with the surface was measured. Three areas (10 μm × 10 μm) were analyzed, and the average value is reported. The data obtained should be considered as semiquantitative (especially for the thinnest layers), showing tendency rather than absolute values. The reason for the semiquantitative character of the data originates in the relatively high polydispersity of the nanoparticles used.

In fact, the measurement of the image depth indicated that the total distance from the peak to the surface gradually decreases as the thickness of the PVP film increases (Figure 9). For a film thickness between 3 and 10 nm, the measured average bearing depth is in the range of 170−180 nm, which is in agreement with the previously measured particle size
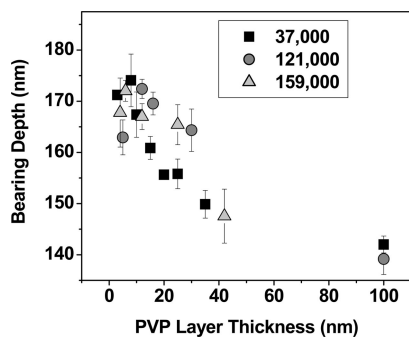
FIGURE 9. Bearing depth (determined from AFM imaging and indicating the level of incorporation of the particles in the PVP layer) versus the thickness of the PVP layer.
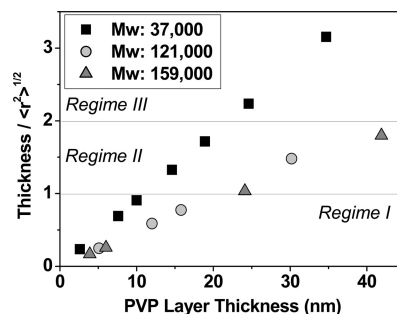

FIGURE 10. Ratio between the thickness of the PVP layer and the unperturbed end-to-end distance of the PVP macromolecules versus the thickness of the PVP layer.

(128 ± 54 nm). With an increase of the PVP film thickness, the distance between the peak and the surface gradually decreases, indicating that the particles are sunk deeper into the PVP film. These results confirm the above hypothesis and clearly prove that the contact area between the particles and the PVP film increases with an increase in the film thickness, resulting in a higher force. Penetration of the particles into the layer is estimated to be between 1−3 nm [for the thinnest (2−5 nm) layers] and 30−40 nm [for the thicker (∼40 nm) layers].

Strength of the Adhesive Bond. As was already indicated, the penetration of the particles into the layer is estimated to be between 1−3 and 30−40 nm. Thus, the contact area between a nanoparticle and the bonding polymer layer can be estimated by the following equation for the surface of a spherical cap (hemisphere):

$$S = \pi DH \qquad (14)$$

where D is the diameter of an average nanoparticle (128 nm) and H is the segment height (penetration depth). The contact area is between 400−1200 nm^2 (for the thinnest layers) and 12000−16000 nm^2 (for the thicker layers). Next, the strength of the adhesive joint, Ad, can be evaluated by employing data from Figure 8 and taking the lowest force value (needed to destroy the joint) for the thinnest layers ($\mathbf{P} \sim \mathbf{N}_n \sim \mathbf{F}_y = 55$ nN) and the highest measured value (needed to destroy the joint) for the thick (∼40 nm) layers ($\mathbf{P} \sim \mathbf{N}_n \sim \mathbf{F}_y = 290$ nN). We now introduce the ratio $\mathbf{P}/\mathbf{F}_y = R$ as a characteristic constant for a polymer bonding layer/particle assembly with a certain thickness of the polymer layer and a value of the penetration depth, H. We denote this ratio for the thinnest layers as $R = R_1$ and for the thicker layers as $R = R_2$. Because the coefficient of proportionality between $\mathbf{P}$ and $\mathbf{F}_y$ is not yet identified numerically, the ratio R allows us to perform an assessment of the influence of the PVP layer thickness on the strength of the adhesive bond, Ad.

When the data for contact area S for the thinnest bonding layers are substituted in (4), the strength of the adhesive bond is estimated as $45R_1$ MPa $< Ad_1 < 138R_1$ MPa. Accordingly, the strength of the adhesive joint for the thicker layers is estimated as $18R_2$ MPa $< Ad_2 < 24R_2$ MPa. It should be noted that, according to the phenomenological mechanical

model (13), R_2 is smaller than R_1 if the friction coefficient K is a constant (which is true in our case for the contact between the cantilever tip and the silica nanoparticle). From the obtained data, it is evident (at least on a semiquantitative level) that the strength of the adhesive joint, Ad, increases with a decrease in the thickness of the polymer bonding layer. In addition, it has to be pointed out that $Ad_1 \neq Ad_2$ even if $R_1 = R_2$. Therefore, the mechanical model alone cannot explain the relationship between the strength of the adhesive bond and the PVP layer thickness. We hypothesize that variations in the inherent properties of the polymer bonding layers with the thickness cause the observed dependency. In other words, in addition to the mechanical arguments, the layer molecular structure is responsible for the observation that the strength of the adhesive joint increases with a decrease in the thickness of the layer.

Molecular Characteristics of the PVP Bonding Layer. Depending on the layer thickness, several cases of organization of the ultrathin adhesive joint can be considered. The cases are suggested by the ratio A between the size of the PVP macromolecule (unperturbed end-to-end distance) and the layer thickness. The root-mean-square end-to-end distance for the PVP macromolecules can be estimated from the following equation (21):

$$\langle r^2 \rangle^{1/2} = a(N)^{1/2} \qquad (15)$$

where a is the statistical segment length and N is the degree of PVP polymerization. The statistical segment length for PVP was assumed to be 0.6 nm, the same as that reported for polystyrene (22). The end-to-end distances are 11, 20.4, and 23.3 nm for PVPs with molecular weights of 37 000, 121 000, and 159 000 g/mol, respectively. The ratio between the layer thickness h and $\langle r^2 \rangle^{1/2}$ versus the thickness of the layer is plotted in Figure 10.

At least three regimes of macromolecular arrangement in the bonding layer can be distinguished. The first regime corresponds to the case of the macromolecular monolayer where the thickness of the layer is lower than the size (end-to-end distance) of the polymer chain ($A < 1$). In this scenario, each macromolecule contacts both the substrate and the particle to be joined. When $1 < A < 2$, different macromolecules contact the particle and substrate (regime II). However, all macromolecules in the layer are still in
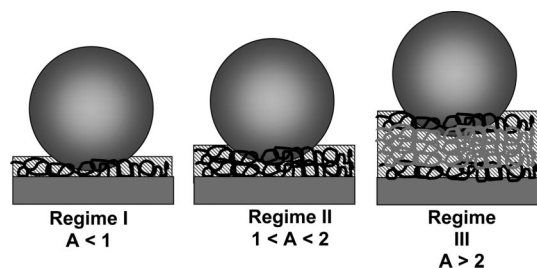
FIGURE 11. Three different regimes of arrangement of PVP macromolecules in the bonding layer. The sketch is not to scale: the thickness of the bonding layer and the sizes of the macromolecules are exaggerated.

contact with the surface. These macromolecules, contacting different surfaces, are also entangled between themselves. In the third regime $A > 2$, there are polymer chains in the layer that do not come into direct contact with the surface. With increasing layer thickness, the number of these "noncontacting" macromolecules increases. All of these regimes are depicted schematically in Figure 11.

The level of the chain's entanglement in the PVP bonding layer is determined by the degree of polymerization of the polymer molecules. To form stable entanglements the molecular weight of the macromolecules in a material should be comparable with or higher than the critical entanglement molecular weight, M_C. The M_C value for PVP chains has to be very close to the M_C value for polystyrene ($M_C = 31\ 200$ g/mol (21)) which has a chemical structure very similar to that of PVP. Therefore, all PVP macromolecules used in this work have molecular weights higher than M_C and can, thus, form stable entanglements in the bonding layers.

Molecular Characteristics of the PVP Bonding Layer and the Strength of the Adhesive Bond. In our experiment, we observed cohesive failure of the adhesive joint between the PVP layer and silica nanoparticles. As known from the scientific literature, the cohesive energy for PVP is estimated as 45 000 J/mol (23). Because the molar volume of the vinylpyridine unit is 92×10^{-6} m^3/mol, the cohesive energy for PVP is estimated as 5×10^{-4} MPa. The strength of an adhesive joint measured in this work is much higher than the cohesive energy for the PVP material. However, it is typical for polymers that the stresses needed to break down the materials are several orders of magnitude higher than the value estimated from the cohesive energy (22). For instance, the fracture stress for the bulk of glassy polystyrene is reported to be 41 MPa (23). This value is the same order of magnitude as the stresses reported here for the ultrathin films destroyed during the measurement of the strength of the adhesive bond.

One of the major reasons that polymers demonstrate higher (than predicted by the cohesive energy) values of break-down stresses is due to the additional work needed on the molecular level for chain straightening (rubber elasticity effects), chain scission (breakage of chemical bonds), and chain pull-out (chain separation) (22, 24). The pull-out work for the fracture formation requires significantly less energy compared to the one needed for the chain scission. For long, highly entangled chains or chain fragments, there

is significant fraction of chain-scission events. For shorter, less entangled chains/chain fragments, there is mostly a pull-out mechanism in effect.

For the thin polymer bonding layers studied in the present work, the competition between pull-out and chain-scission mechanisms may decide the overall strength of the adhesive joint. For very thin layers (regime I, Figure 11), a single polymer chain is strongly anchored to the particle and to the substrate. Because no particle delamination was observed, the chain scission accompanied by chain straightening is the most probable mechanism for the breakdown. As the thickness of the PVP layer increases (regimes II and III), more pull-out events can contribute to the certain reduction of the strength of the adhesive joint. This work is in progress, and at the current stage, we are unable to clearly discriminate between the regimes II and III and polymers possessing different molecular weights, as well as between chain-scission and pull-out mechanisms. However, the obtained data show that the proposed method, with further improvement, allows quantitative characterization of the strength of ultrathin adhesive joints.

CONCLUSIONS

It was demonstrated that the strength of the adhesive joint between silica nanoparticles and ultrathin PVP bonding layers (with the thickness between 3 and 100 nm) can be tested using the tip of the AFM cantilever. Specifically, the strength of the adhesive joint was probed in a tearing contact mode, when the particle was removed by applying a tangential force parallel to the substrate surface. It was found that the particles are removed by destroying the cohesive contact zone and that the PVP thickness had a pronounced effect on the force needed to destroy the adhesive joint. In particular, the greater the film thickness, the larger is the required break force. However, the strength of the adhesive joint was estimated to be higher for a thinner layer. It is suggested that mechanical properties of the system as well as molecular characteristics of the PVP layer are responsible for the trend observed. In this experimental study, the molecular weight of the polymer did not significantly affect the strength of the adhesive joint.

REFERENCES AND NOTES

(1)   Baldan, A. *J. Mater. Sci.* **2004**, *39*, 4729.
(2)   Goss, C. A.; Charych, D. H.; Majda, M. *Anal. Chem.* **1991**, *63*, 85.
(3)   Chumanov, G.; Sokolov, K.; Cotton, T. M. *J. Phys. Chem.* **1996**, *100*, 5166.
(4)   Brayner, R.; Viau, G.; Bozon-Verduraz, F. *J. Mol. Catal. A: Chem.* **2002**, *182*, 227.
(5)   Malynych, S.; Luzinov, I.; Chumanov, G. *J. Phys. Chem. B* **2002**, *106*, 1280.

(6) Iyer, K. S.; Moreland, J.; Luzinov, I.; Malynych, S.; Chumanov, G. In *Film Formation. Process and Morphology*; Provder, T., Ed.; ACS Symposium Series 941; American Chemical Society: Washington DC, 2006; Chapter 11, p 149.

(7) Sheehan, P. E.; Lieber, C. M. *Science* **1996**, *272*, 1158.

(8) Junno, T.; Deppert, K.; Montelius, L.; Samuelson, L. *Appl. Phys. Lett.* **1995**, *66*, 3627.

(9) Baur, C.; Bugacov, A.; Koel, B. E.; Madhukar, A.; Montoya, N.; Ramachandran, T. R.; Requicha, A. A. G.; Resch, R.; Will, P. *Nanotechnology* **1998**, *9*, 360.

(10) Junno, T.; Anand, S.; Montelius, L.; Samuelson, L. *Appl. Phys. Lett.* **1995**, *66*, 3295.

(11) Eppler, A. S.; Rupprechter, G.; Anderson, E. A.; Somorjai, G. A. *J. Phys. Chem. B* **2000**, *104*, 7286.

(12) Yang, D.-Q.; Sacher, E. *Appl. Surf. Sci.* **2003**, *210*, 158.

(13) Boyd, R. D.; Verran, J.; Jones, M. V.; Bhakoo, M. *Langmuir* **2002**, *18*, 2343.

(14) Senechal, A.; Carrigan, S. D.; Tabrizian, M. *Langmuir* **2004**, *20*, 4172.

(15) Pocius, A. V. *Adhesion and Adhesive Technology*, 2nd ed.; Hanzer Publishers: Munich, Germany, 2002; p 44.

(16) *Scanning Probe Microscopy Training Book*; Digital Instruments, Veeco Metrology Group: Plainview, NY, 2000.

(17) Tottonese, M.; Kirk, M. *SPIE Proc. Ser.* **1997**, *3009*, 53.

(18) Johnson. K. L. *Contact Mechanics*; Cambridge University Press: Cambridge, U.K., 1987.

(19) Bowden F. P.; Tabor, D. *The Friction and Lubrication of Solids*; Oxford University Press: Oxford, U.K., 1986.

(20) Ling, J. S. G.; Leggett, G. J.; Murray, A. J. *Polymer* **1998**, *39*, 5913.

(21) Iyer, K. S.; Luzinov, I. *Macromolecules* **2004**, *37*, 9538.

(22) Sperling, L. H. *Polymeric Multicomponent Materials*; John Wiley & Sons Inc.: New York, 1998.

(23) Bicerano, J. *Prediction of Polymer Properties*; Marcel Dekker: New York, 2002.

(24) Wool, R. P. *Polymer Interfaces: Structure and Strength*; Hunser/ Gardner: New York, 1995.